Stability of flow and the transition to turbulence around a quartz tuning fork in superfluid ^{4}He at very low temperatures

D. I. Bradley, M. J. Fear, S. N. Fisher, A. M. Guénault, R. P. Haley,* C. R. Lawson, G. R. Pickett, R. Schanen,† V. Tsepelin, and L. A. Wheatland

Department of Physics, Lancaster University, Lancaster LA1 4YB, United Kingdom

(Received 11 February 2014; revised manuscript received 15 April 2014; published 9 June 2014)

We have studied the transition between pure potential flow and turbulent flow around a quartz tuning fork resonator in superfluid ^{4}He at millikelvin temperatures. Turbulent flow is identified by an additional drag force on the fork prongs due to the creation of quantized vortices. When driven at a constant driving force amplitude, the transition to turbulence causes an abrupt decrease in the velocity amplitude of the prongs. For a range of driving forces, continuous switching is observed between the two flow states. We have made a statistical study of the switching characteristics and of the lifetimes of the unstable states. We find a characteristic velocity $v^\star$ which separates quasistable turbulent flow at higher velocities and quasistable potential flow at lower velocities. We show that the potential-to-turbulent flow transition is driven by random processes involving remanent vortices pinned to the prongs.

DOI: 10.1103/PhysRevB.89.214503 PACS number(s): 67.25.dk, 67.25.dg, 47.27.Cn

I. INTRODUCTION

In recent years tuning fork resonators have found a wide variety of applications in quantum fluids and solids research. They have been used to measure viscosity [1–3], turbulence [4,5], cavitation [6], Andreev scattering [7,8], acoustic modes [9–11], and the mechanical properties of solid helium [12].

When a tuning fork is immersed in a fluid, the motion of the prongs produces backflow of the fluid. Here the fluid is liquid ^{4}He at temperatures below 10 mK, so that it is essentially a pure superfluid. At low velocities the backflow of the superfluid is pure potential flow with no dissipation. At higher velocities the pure potential flow becomes unstable, quantum vortices are generated, and dissipation occurs. This causes drag on the prong motion which is observed as increased damping of the fork resonance. This type of behavior was first observed using vibrating spheres [13] and vibrating wire resonators [14,15]. We refer to the resulting flow as "turbulent," although fully developed quantum turbulence, corresponding to a large scale vortex tangle [16], may require much higher velocities. Below we describe experiments using commercially available miniature quartz tuning forks [17] to study the transition between the pure potential flow and turbulent flow states in the zero temperature limit.

In a typical experiment the amplitude of the driving force is incremented in small steps while we measure the velocity amplitude of the prong tips. In the pure potential flow state the velocity is found to be accurately proportional to the driving force. Here the small damping arises from the intrinsic properties of the fork. Above a critical velocity amplitude the pure potential flow state becomes unstable and at some time later an abrupt transition occurs to the turbulent state. The increased damping reduces the velocity amplitude of the fork prongs and the velocity-force response becomes nonlinear. The two states are easily distinguished by their different force-velocity relationships, which are highly reproducible. However, the transition itself is highly irreproducible and hysteretic [5,18]. Similar behavior has been observed with vibrating wires [14,19,20] and vibrating spheres [13]. For a narrow range of driving force amplitudes the flow around the tuning fork switches continuously between the potential flow and turbulent flow states. At higher driving force amplitudes a single transition is observed from potential flow to turbulent flow, and at lower driving force amplitudes a single transition is observed from turbulent flow back to potential flow. We present a detailed statistical study of the velocities at which these transitions occur, and we compare our data with previous measurements on vibrating spheres [21–23].

In Sec. II we describe the experimental arrangement and measurement techniques. In Sec. III we present measurements of the velocity-force response, showing the transition between the potential flow and turbulent flow states. In Sec. IV we investigate the continuous switching regime and in Sec. V we investigate transitions outside of the continuous switching regime. In Sec. VI we summarize our results and suggest a qualitative explanation based on the behavior of remanent vortices.

II. EXPERIMENT

A schematic of the experimental cell is shown in Fig. 1. The cylindrical cell wall is made of epoxy resin. The ^{4}He sample is cooled by silver-sintered heat exchangers connected via a high purity annealed silver wire to sinters in the mixing chamber of a dilution refrigerator. A heater on the wire and a thin film RuO_2 resistance thermometer inside the cell allow for temperature measurement and regulation. In these experiments, the ^{4}He sample was "dewar helium" and thus contains a small concentration of ^{3}He impurities. All the data presented here were taken at a pressure of 1 bar and

*r.haley@lancaster.ac.uk
†r.schanen@lancaster.ac.uk

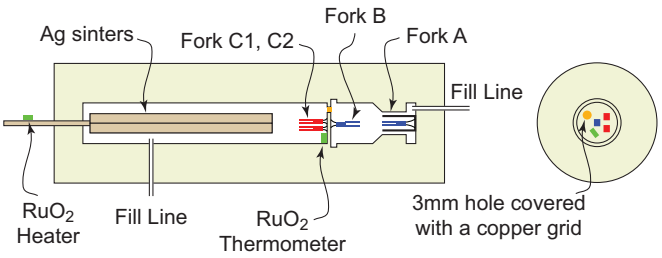

FIG. 1. (Color online) The experimental cell contains four identical forks [17]. The measurements reported here were made on fork A. Most of the volume is occupied by the silver sinter heat exchangers used to cool the ^{4}He sample.

at temperatures below 10 mK where there is negligible normal fluid.

Measurements of the flow transitions were made on fork A, shown in Fig. 1. The neighboring fork B was used to induce transitions on fork A for some of the experiments described in Sec. V. Fork B has a small piece of Kapton foil glued to the top of each prong to help promote vortex generation. Forks A and B are partitioned from the bulk of the cell which contains the sinters and two further tuning forks which were not used in the experiments described here. The forks have nominally identical dimensions with prongs of length $L = 3.34$ mm, thickness $T = 450$ μm, and width $W = 450$ μm, and are designed to resonate at a fundamental frequency close to 32.768 kHz in vacuum. In superfluid helium at low temperatures fork A has a resonant frequency of 31.7 kHz and a quality factor of 6×10^5, while the Kapton attached to fork B reduces the resonant frequency to 31.4 kHz and the quality factor to 2×10^4.

The tuning fork is excited at its resonant frequency with a driving voltage of amplitude V supplied by a waveform generator with suitable attenuators. The amplitude of the driving force on each prong is given by [2]

$$F = aV/2, \tag{1}$$

where a is the fork constant. The motion of the prongs generates a current of amplitude I which is measured using a custom-made current-to-voltage converter [24] and a two-phase lock-in amplifier referenced to the generator. The velocity amplitude of the prong tips v is found using the fork constant

$$v = I/a. \tag{2}$$

The fork constant is estimated from the characteristics of the resonance at low velocities [10],

$$a = \sqrt{\frac{4\pi m_{\rm eff}\,\Delta f_2\, I_r}{V}}, \tag{3}$$

where Δf_2 is the width of the resonance, I_r is the current amplitude at the resonant frequency, V is the amplitude of the driving voltage, and the effective mass of the prongs in vacuum is $m_{\rm eff} = \rho LTW/4$, where ρ is the density of quartz. From this we determine the fork constant for fork A to be $a = 12$ μC m^{-1}. Direct optical measurements [25] on similar forks show that the true fork constant agrees with the electromechanical estimate to within about 10%.

At the resonant frequency, the velocity of the prongs is exactly in phase with the driving force. In this case the inertial and restoring forces on the prongs exactly cancel so the damping force is equal to the driving force. In practice the resonant frequency depends on the velocity, so to measure the velocity versus damping force response accurately we use a computer-controlled-continuous tracking routine to keep the fork on resonance. The routine adjusts the driving frequency until the out-of-phase signal (which is zero at resonance) becomes less than a small fraction (usually 1%) of the in-phase signal.

III. FORCE-VELOCITY RESPONSE

Figure 2 shows the tip velocity amplitude versus the amplitude of the driving force, which is equal to the dissipative drag force. These results were briefly reported earlier [18]. The points in the figure show the locations of the flow transitions for many sweeps of the driving force. In each sweep the driving force is first increased from 13.5 to 19.0 nN in 200 equally spaced steps. There is a settling time, usually 5 s, after each drive adjustment to allow the fork to stabilize. Each reading may take multiples of the settling time if the drive frequency requires adjustment to maintain resonance. In practice, little frequency adjustment is required except immediately following the transition. If the transition produces a large velocity change, then several adjustments are required before resonance is restored. On reaching the maximum driving force, the end of the upsweep, the driving force is then decreased back to 13.5 nN using the same steps. A

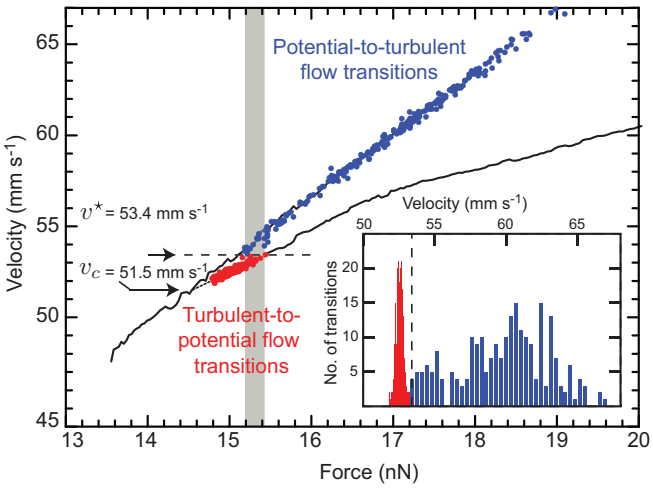

FIG. 2. (Color online) The solid line shows the velocity-force response of fork A in superfluid ^{4}He at very low temperatures. The data points show the locations of transitions for many different sweeps. Each point indicates the velocity immediately before a transition: blue for transitions from potential flow to turbulent flow during an upsweep; red for transitions from turbulent flow to potential flow during a downsweep. The inset shows a histogram giving the distribution of velocities at which the transitions occurred. Regions of the two different unstable flow states are bounded by a characteristic velocity $v^\star = 53.4$ mm s^{-1}. In the intermediate driving force region, shaded gray, the flow continuously switches back and forth between the two flow states.

typical up-down cycle takes 1–2 h. We took the measurements overnight for several weeks to collect sufficient data.

Figure 2 has two points for each up-down cycle. The points at higher velocities (blue online) show the tip velocity amplitude in the pure potential flow state immediately before the potential-to-turbulent flow transition during the upsweep. The points at lower velocities (red online) show the tip velocity amplitude in the turbulent flow state immediately before the turbulent-to-potential flow transition during the downsweep.

The solid line in Fig. 2 shows the full response curve measured by a single up-down cycle which went up to a larger driving force. For this particular sweep, the potential-to-turbulent flow transition occurred at $v \approx 60$ mm s^{-1} on the upsweep and the turbulent-to-potential flow transition occurred at $v \approx 53$ mm s^{-1} on the downsweep. We define the critical velocity for turbulence v_c as the velocity at which the extrapolated turbulent response curve joins the potential response curve (i.e., it is the velocity at which the turbulent drag extrapolates to zero). For fork A we find $v_c = 51.5$ mm s^{-1}.

Referring to Fig. 2 we see that the potential flow state appears to be stable for velocity amplitudes below $v^\star = 53.4$ mm s^{-1} since we have not observed any transitions to the turbulent flow state below this velocity. Conversely, the turbulent state appears to be stable above $v^\star$ since we have not observed any transitions to the potential flow state above this velocity. There exists a range of driving forces, shown by the shaded region in Fig. 2, where both flow states are unstable and the prong tip velocity flips continuously between the upper and lower response curves as the flow switches between the two states. An example of this behavior is shown in Fig. 3. Similar behavior has been observed in vibrating sphere experiments [21].

The inset to Fig. 2 shows a histogram of the number of times a transition was observed versus the prong tip velocity before the transition. The distribution of potential-to-turbulent flow transitions during the upsweep has a broad maximum at ≈60 mm s^{-1}, while the distribution of turbulent-to-potential flow transitions during the downsweep is much narrower with a peak at ≈52.6 mm s^{-1}.

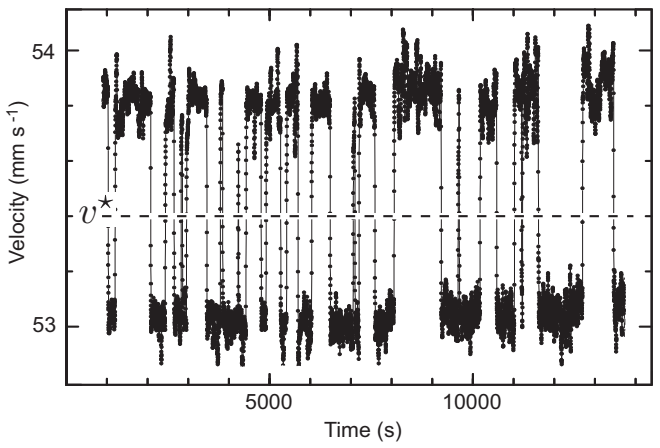

FIG. 3. The prong tip velocity amplitude vs time at a constant driving force amplitude in the intermittent regime. The velocity flips spontaneously either side of $v^\star$ between the potential (high velocity) and turbulent (low velocity) flow states.

The velocity $v^\star$ plays a very significant role. It gives a boundary between quasistable potential flow below $v^\star$ and quasistable turbulent flow above $v^\star$. We use the phrase "quasistable" here to mean that we have never observed transitions out of these flow states. However, we cannot be sure that transitions would not have occurred if we had waited for an indefinite length of time. We discuss this in more detail in Secs. V and VI. For velocities higher than $v^\star$ the potential flow state is unstable and for velocities below $v^\star$ the turbulent flow state is unstable. This results in an intermittent region of continuous switching, shown by the shaded region in Fig. 2. Here the driving force amplitude is such that the velocity in the potential flow state exceeds $v^\star$, so the potential flow state is unstable, while the velocity in the turbulent flow state is below $v^\star$, so the turbulent flow state is also unstable. This results in spontaneous switching between the two flow states. The statistical properties of this are analyzed in the following section.

IV. INTERMITTENT REGION

We made a detailed study of the switching statistics close to the center of the intermittent region at a driving force of 15.3 nN. The velocity response was measured continuously over a period of nearly 3 days. A portion of the data is shown in Fig. 3. The velocity oscillates between two values on either side of $v^\star$: $v \approx 53.1$ mm s^{-1} in the turbulent flow state and $v \approx 53.9$ mm s^{-1} in the potential flow state. Under these conditions each unstable flow state lasts for a time period ranging from a few seconds up to almost 1 h.

We performed a statistical analysis as follows. First we extracted the length of time that the flow survives in a given state before making the transition to the other state. This gives two sets of data, each with about 400 survival times, one for the potential flow state and one for the turbulent flow state. For each flow state we define $n(t)$ as the number of states which have lifetimes exceeding time t. The decay rate can be written as

$$\frac{dn}{dt} = -\lambda n, \tag{4}$$

where $\lambda = 1/\tau$ is the transition probability per unit time and τ is the corresponding mean lifetime. If λ is independent of time, then we have an exponential decay

$$n(t) = n(0)\exp(-t/\tau). \tag{5}$$

In Fig. 4 we plot the probability $n(t)/n(0)$ that a given flow state has a lifetime exceeding t, versus the time t. We show this for both the potential flow and the turbulent flow states. The solid lines in the figure show fits to the exponential decays, Eq. (5), with mean lifetimes $\tau_P = 400 \pm 4$ s for the pure potential flow state and $\tau_T = 225 \pm 2$ s for the turbulent flow state.

The data for the turbulent flow state accurately follow the exponential decay law, showing that the turbulent-to-potential transition is governed by a random process, i.e., the transition probability λ is independent of time. This was also found to be the case for turbulent flow around an oscillating sphere [22].

The potential flow state also shows convincing exponential behavior at early times, indicating that the potential-to-turbulent transition is also governed by a random process.

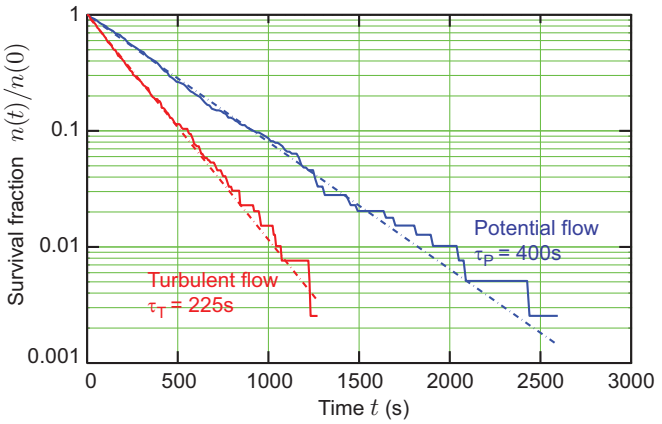

FIG. 4. (Color online) Lifetimes in the intermittent region. The log-linear plot shows the fraction of flow states remaining without transition after a time t. The lines show fits to simple exponential decays with average lifetimes τ.

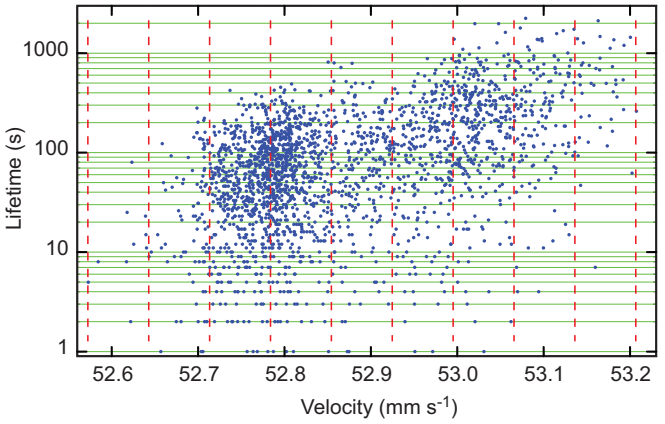

FIG. 6. (Color online) Survival times in the turbulent unstable state. The time of each event is plotted at its average velocity. The vertical lines show the boundaries of the nine velocity bins chosen to investigate the velocity dependence.

However, at longer times, $t \gtrsim 1500$ s, the data lie higher than the fitted line, indicating that the mean lifetime increases for longer-lived potential flow states. We believe that this results from a reduction in the density of mobile remanent vortices attached to the prongs. This is discussed further in Sec. VI.

V. SURVIVAL TIMES IN THE UNSTABLE STATES

On increasing drive in the intermittent region, as the velocity in the turbulent state approaches $v^\star$, the fork spends an increasing proportion of time in the turbulent flow state and the lifetime of the turbulent flow state increases. In order to make a detailed study of the velocity dependence we have developed techniques to prepare the flow in a given state.

A. Turbulent flow state

To prepare an unstable turbulent state we use the technique illustrated in Fig. 5. First we adjust the drive on fork A to give a velocity above the critical velocity v_c, in the quasistable potential flow state. Then we drive the nearby fork B above its critical velocity to create turbulence. Fork A detects the presence of turbulence by entering the turbulent state. A similar scheme has been used to detect vortex emission from quantum turbulence created by vibrating wires [26]. After this the drive to fork B is switched off and the turbulent state of fork A becomes unstable. We continue to track fork A to measure its average velocity in the turbulent flow state and the time elapsed before it makes the transition back to the potential flow state. In order to gather sufficient data for reliable statistics, this was repeated many times and at several different velocities using an automated computer program. The measurements were recorded over several days.

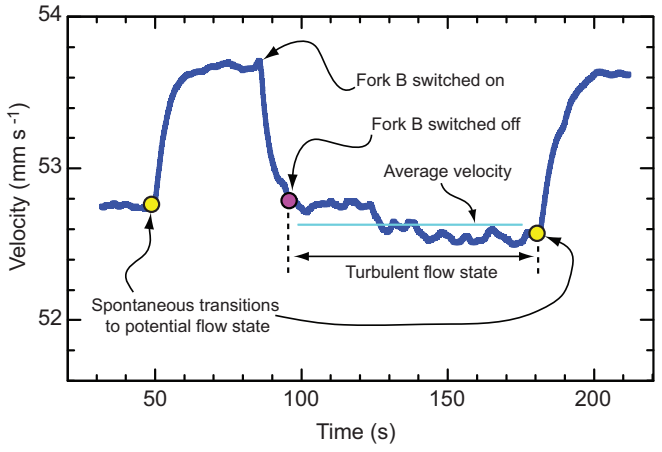

FIG. 5. (Color online) Preparing the unstable turbulent flow state. The plot shows the prong tip velocity of fork A vs time. A brief excitation of nearby fork B induces the turbulent flow state around fork A.

Figure 6 shows the lifetime of each turbulent state versus the average velocity in the turbulent state. The lifetimes span more than three orders of magnitude. To investigate the statistical properties we have grouped the data into nine velocity bins, indicated in Fig. 6 by the vertical dashed lines. In Fig. 7 we plot for each bin the fraction of the turbulent states which survive, $n(t)/n(0)$, versus the time t elapsed from preparation (taken to be the time at which the drive to fork B is removed). The data fit very well to exponential decays, Eq. (5), indicating that the collapse of the turbulent state is governed by a random process.

Figure 8 gives the fitted values of the average lifetime of the turbulent flow state τ_T versus the prong tip velocity amplitude. The average lifetime increases very rapidly, by a factor of ~40, as the velocity increases from $v = 52.6$ to 53.2 mm s^{-1}. The figure also shows the average lifetime of the turbulent flow state obtained from the spontaneous switching data in Fig. 4. This agrees well with the measurements for the prepared states, which indicates that the turbulent flow state is the same in the two cases.

The average lifetimes of the turbulent flow state fit reasonably well to a simple exponential,

$$\tau_T = \tau_0 \exp[(v - v_c)/v_0], \tag{6}$$

where $\tau_0 = 0.02$ s and $v_0 = 0.16$ mm s^{-1} are fitting parameters, shown by the straight line in Fig. 8. The data also fit well

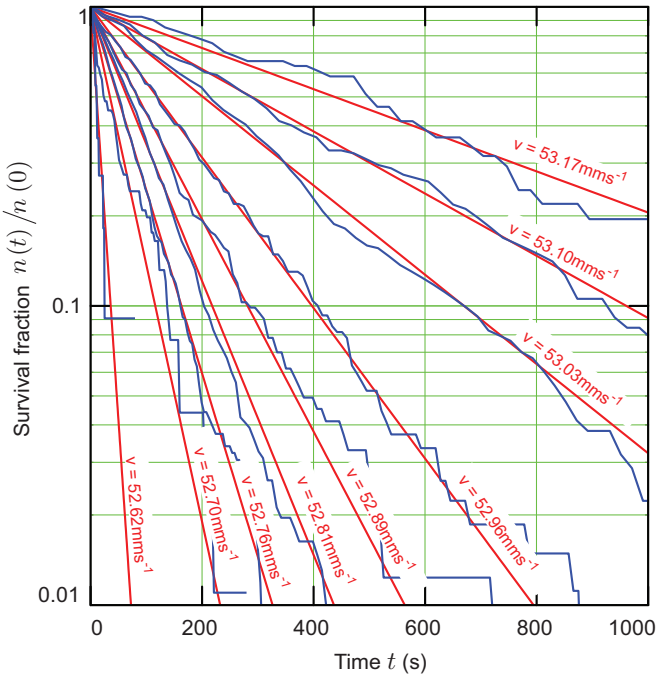

FIG. 7. (Color online) The fraction of turbulent flow states $n(t)/n(0)$ remaining vs the elapsed time t since their formation, for each of the nine velocity bins shown in Fig. 6. Data in each of the bins fit well to an exponential decay indicated by the solid lines.

to a form used by Schoepe [23] to fit data from oscillating sphere measurements,

$$\tau_T = \tau_1 \exp\{[(v - v_c)/v_1]^2\}, \quad (7)$$

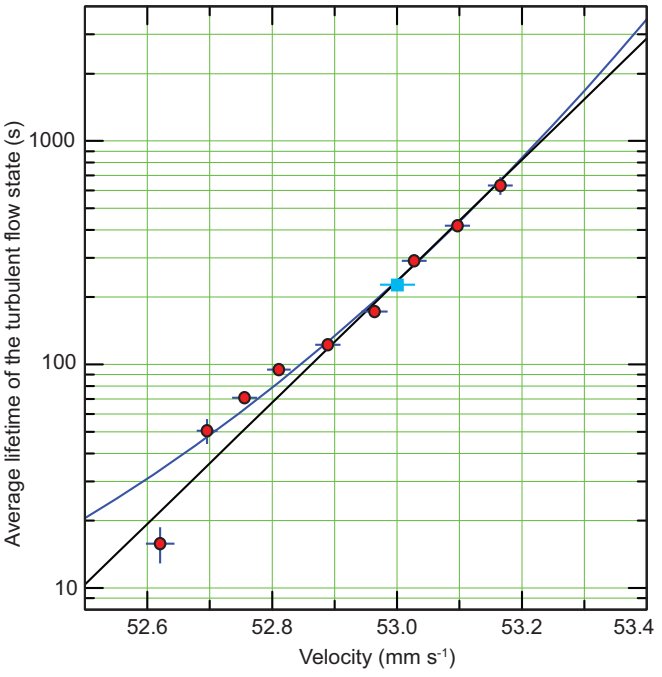

FIG. 8. (Color online) The average lifetime τ_T of the turbulent flow state vs the prong tip velocity amplitude. Circles show values obtained from the fitted lines in Fig. 7. The square shows the fitted value from the intermittent switching region discussed in Sec. IV.

where $\tau_1 = 3$ s and $v_1 = 0.72$ mm s^{-1} are fitting parameters, shown by the curved line in Fig. 8. The value of v_1 is roughly twice the value used to fit the vibrating sphere data.

Neither of the expressions for τ_T given above have a divergence at $v^\star$, which suggests that the turbulent flow is not absolutely stable at higher velocities. A more definitive test of this would require measurements much closer to $v^\star$.

B. Pure potential flow state

In this section we present measurements of the potential-to-turbulent flow transitions for a range of velocities above $v^\star$. The preparation technique is illustrated in Fig. 9. This was found empirically to be the most successful method of preparing potential flow states, as discussed below in Sec. VI C. Starting in the turbulent flow state, the drive to fork A is first turned off to recover the potential flow state. (The oscillation around zero velocity in Fig. 9 immediately after removing the drive is due to the ringdown of the fork motion beating with the reference frequency of the measurement lock-in amplifier.) After a waiting time of 10 min or so, the fork is driven in the stable potential flow region at a velocity close to v_c. The drive is then increased slowly to give a velocity in the unstable potential flow regime with $v > v^\star$. The drive then remains constant while we monitor the fork velocity to observe the transition to the turbulent flow state. The transition is clearly identified by a sudden drop in velocity, as shown in the figure. We measure the lifetime of the unstable potential flow state from the time of preparation, i.e., from the time at which the drive is held constant, as indicated in Fig. 9.

The measured lifetimes of the pure potential flow state are shown in Fig. 10. Unfortunately there are insufficient data to test whether the survival times obey an exponential decay law as we did for the turbulent flow state in Sec. V A. Nevertheless, we can group the data in bins to estimate the average survival times at various velocities, as shown in Fig. 11. The data are sparse, but sufficient to suggest that the survival times increase

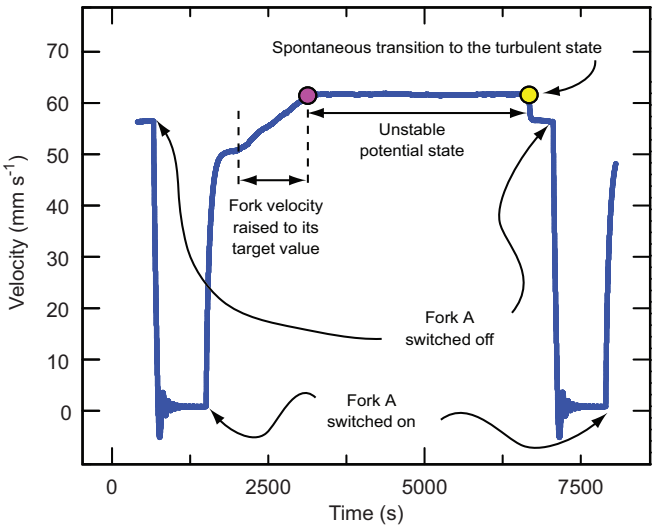

FIG. 9. (Color online) Preparing the unstable potential flow state. The plot shows how the prong tip velocity of fork A was controlled and monitored over time (see text).

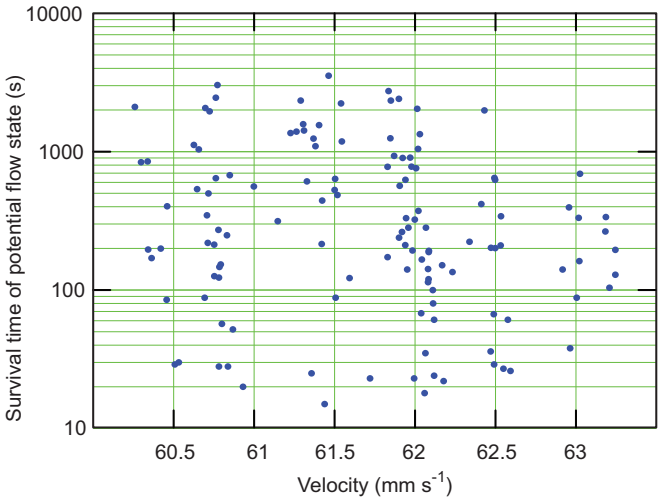

FIG. 10. (Color online) Lifetimes of unstable pure potential flow states vs the amplitude of the prong tip velocity.

rapidly with decreasing velocity, varying from about 200 s at 63 mm s^{-1} to around 700 s at 60.5 mm s^{-1}.

We also attempted to make measurements of the lifetime of the potential flow state at a much lower velocity of $v = 55.9$ mm s^{-1}. However, often we would find no transition after several hours and we were not able to gather sufficient data for statistics. Instead, we investigated the reduction of the survival time by the presence of vortices generated by the neighboring fork B, similar to measurements made previously using vibrating wires [26]. Several overnight measurement series were made under automated computer control. Fork A was first set in the potential flow state at a velocity of 55.9 mm s^{-1}. Then fork B was driven to some chosen velocity above its critical velocity, while monitoring fork A to find the resulting lifetime of the potential flow state. When fork B was driven at high velocities, the potential flow state around fork A was very short lived. On decreasing fork B velocity, the average lifetimes lengthened dramatically from seconds to hours. For the lowest measured velocity of fork B, we

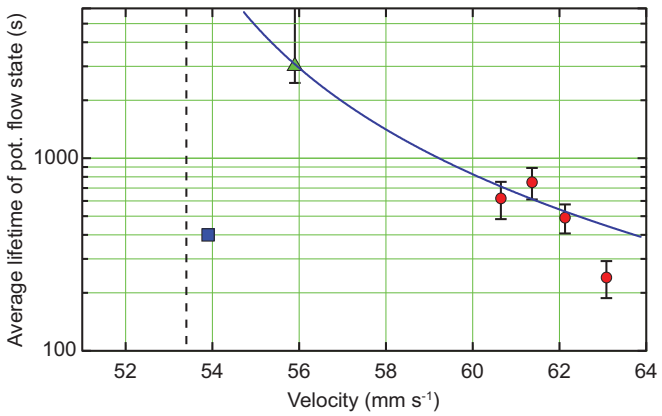

FIG. 11. (Color online) Average lifetimes of the pure potential flow state τ_P vs velocity v. Round points give the average lifetimes for the prepared states in Fig. 10. The triangle is a lower bound described in Sec. V B. The dashed line shows the velocity $v^\star = 53.4$ mm s^{-1}. The square shows the value from the intermittent switching region discussed in Sec. IV.

observed the transition of 20 potential flow states around fork A. Their survival times ranged from several minutes to several hours with an average of around 3000 s. We take this to be an approximate lower bound for the average lifetime time of the undisturbed potential flow state at this velocity, shown in Fig. 11.

The data are not sufficient to determine the exact functional form of τ_P. As a guide to the eye, the solid line in Fig. 11 shows a fit to

$$\tau_P = \tau_2 \left(\frac{v_c}{v - v_c} \right)^2, \tag{8}$$

where $\tau_2 = 23$ s is a fitting parameter.

Our measurement in the intermittent switching region from Sec. IV, $\tau_P = 400$ s at $v = 53.8$ mm s^{-1}, is also included in Fig. 11. This shows a much shorter average lifetime than the prepared states at slightly higher velocities. This clearly indicates a history dependence. The lifetime of the potential flow state depends on whether turbulence was generated a short time prior to the measurement. We discuss this further in the next section.

VI. DISCUSSION

A. General features

The flow around the tuning fork can be described by two characteristic velocities $v^\star$ and v_c which define three distinct regions, illustrated in Fig. 12, governed by the fork tip velocity v: (1) For $v < v_c$ there is always stable pure potential flow around the fork with no measurable dissipation. (2) For $v_c < v < v^\star$ the pure potential flow state is quasistable with lifetimes exceeding our typical measurement time of 1 h or more, while the turbulent state is unstable with lifetimes increasing rapidly with increasing velocity. (3) For $v > v^\star$ the turbulent state is quasistable and the pure potential flow state is unstable.

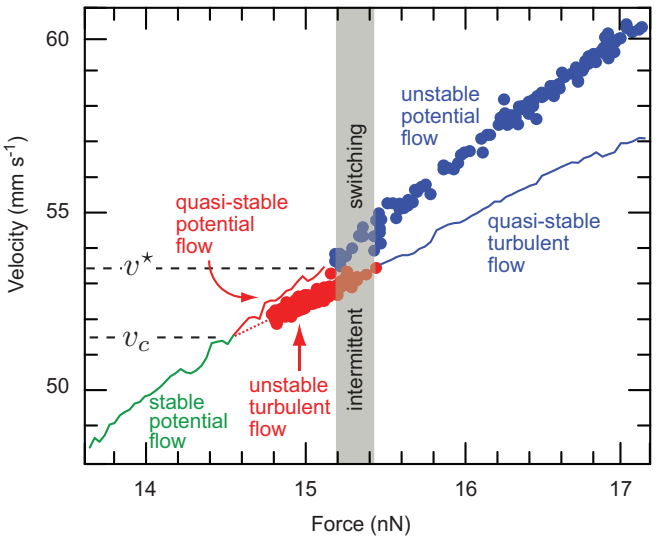

FIG. 12. (Color online) A section of the force-velocity response from Fig. 2 illustrating the three regimes of flow that we have observed: stable pure potential flow for velocities below v_c; quasistable potential flow and unstable turbulent flow between v_c and $v^\star$; quasistable turbulent flow and unstable potential flow above $v^\star$.

The velocity $v^\star$ therefore defines a boundary between different quasistable flow states: pure potential flow below $v^\star$ and turbulent flow above $v^\star$. We have not observed any potential-to-turbulent flow transitions below $v^\star$, nor any turbulent-to-potential flow transitions above $v^\star$. However, we cannot be sure that the flow states are absolutely stable without performing measurements over much longer time periods. Moreover, we note that the fitted exponential expressions for the average lifetime of the turbulent state, Eqs. (6) and (7), do not diverge at $v^\star$.

The velocity $v^\star$ also gives a boundary between *unstable* flow states: unstable turbulent flow for velocities below $v^\star$ and unstable potential flow above $v^\star$. When the fork is driven at a constant driving force amplitude, this naturally results in an intermittent regime where the tip velocity in the pure potential flow is greater than $v^\star$ while the tip velocity in the turbulent flow is less than $v^\star$. In this case the instability of both states means that the flow continuously switches from one to the other.

B. The potential flow to turbulent flow transition

In the region of quasistable turbulent flow indicated in Fig. 12, the potential flow state is unstable. The lifetime of the potential flow state increases rapidly on decreasing velocity, as shown in Fig. 11, except in the intermittent region close to $v^\star$ where the lifetime is significantly shortened. This indicates a strong history dependence. The lifetime of the potential flow state is significantly reduced by the earlier presence of turbulence.

We can understand the behavior by considering remanent vortices. The tuning forks are very rough on the scale of the superfluid coherence length, $\xi \sim 10^{-10}$ m, hence there will be many sites available for vortex pinning, and we propose the following scenario. The nucleation of turbulence requires a remanent vortex to be pinned between suitable pinning sites. The sites should be sufficiently far apart to allow the vortex to grow via the Glaberson-Donnelly instability [27]. The unstable vortex continually grows and twists in the alternating flow, producing vortex rings via self-reconnections. This has been studied in computer simulations [28]. The emitted rings may collide and reconnect to other parts of the oscillating structure, promoting further instabilities and further ring production. This then leads to an avalanche of instabilities and reconnections which drive the flow into the "turbulent" state (we emphasize that the flow is not necessarily fully developed quantum turbulence). The stochastic nature of the transition indicates that the remanent vortices are not static in the potential flow state, but must evolve in time. Vortices may hop from one pinning site to another by tunneling. The tunneling barrier is likely to be reduced by the oscillating flow, so the remanent vortices will evolve faster at larger flow velocities. Thus on increasing velocity in the intermittent region the lifetime of the potential flow state shortens as there is a greater probability of a remanent vortex moving to a suitable pinning site to trigger the transition to turbulent flow.

For velocities just above the intermittent region we find very long lifetimes of the pure potential flow state, as shown in Fig. 11, which are much longer than those observed during intermittent switching measurements. This implies that after waiting for a sufficiently long time the influence of remanent vortices is substantially reduced. Either the vortices decay by shrinking or they find a site where they are strongly pinned and thus become immobile. In either case they are no longer active to trigger the transition to turbulent flow. A direct indication of the reduction of mobile remanent vortices with time is revealed in the late time decay statistics of the potential flow state in the intermittent regime, shown in Fig. 4. The probability λ of the turbulent transition per unit time, given by the slope of the data in Fig. 4, shows a decrease for times exceeding 1500 s. This could be interpreted as a rough estimate of the lifetime of mobile remanent vortices at this particular flow velocity. We expect that this lifetime will become shorter at higher flow velocities as the remanent vortices become more mobile.

For very long times, after the turbulent state ended, the lifetime of the potential flow state might become limited by some other process, such as background ionizing radiation. Evidence for this was found in experiments with oscillating spheres [29], where it was found that the lifetime of the unstable potential flow state is reduced considerably by the presence of a nearby gamma radiation source. Ionizing radiation can produce vortices via the Kibble-Zurek mechanism [30,31]. The resulting vortex rings may collide with the surface of the oscillating object and occupy an unstable pinning site, leading to turbulence in the same manner as suggested above. It is interesting to note that ionizing radiation is also considered as a possible mechanism of the A phase to B phase transition in superfluid ^{3}He at ultralow temperatures [32].

C. The transition to turbulence during drive sweeps

The drive sweep data shown in Fig. 2 can also be understood on the basis of remanent vortices. On increasing drive in the potential flow state the remanent vortices are likely to be quite immobile at first, owing to the low flow velocity and the relatively long time elapsed since the previous turbulent state. In this case the velocity at which the turbulent transition occurs is completely predetermined by the (frozen) distribution of remanent vortices from the previous turbulent state. At higher velocities the remanent vortices become more mobile and the transition to turbulence will develop a stochastic component.

This scenario also explains why the particular preparation technique in Fig. 9 was found to be most effective, since it gives a substantial wait time, ~2000 s, before preparing a new potential flow state. Even using this technique, for every successful preparation of the state there were typically five to ten failures in which the fork made the transition during the preparation process. The failures are likely to have been triggered by the remanent vortices left over from the previous turbulent state. The additional waiting time and the slow ramp to the final velocity helps to anneal the remanent vortices, which leads to a longer lifetime of the potential flow state as well as giving a greater chance that the final velocity is reached without undergoing the transition to turbulence.

D. The turbulent flow to potential flow transition

The lifetime of the turbulent flow state decreases rapidly on decreasing velocity below $v^\star$, as shown in Fig. 8. The underlying processes involved in this transition are likely

to be considerably more complex than the potential flow to turbulent flow transition. In turbulent flow, the tuning fork is moving through a complex and ever-changing network of vortices. In addition, there will be many vortices attached to the surfaces of the fork prongs. Some of these will be pinned while others may be very mobile. In the region of unstable turbulent flow the turbulence is sustained by vortex stretching and vortex reconnections driven by the moving prongs and the surrounding fluid backflow. The local density of the surrounding vortices will fluctuate and one can anticipate that the transition to potential flow, corresponding to the sudden and complete collapse of the turbulent flow, might be triggered by a sufficiently large fluctuation. To explain the behavior of a rough vibrating sphere, Schoepe *et al.* [21,33] speculated that the transition might be triggered by a fluctuation in which the local vortex line density falls to zero. However, a rough surface will cause significant vortex pinning and so it is extremely unlikely that there will ever be a situation where there are no attached vortices. Furthermore, if there was a complete absence of vortices, then the subsequent critical velocity for renucleating the turbulence would be very high, as demonstrated in specially prepared vibrating wire experiments [19], but here we did not observe this. Therefore, in general, the potential flow state around a rough surface must always incorporate a substantial amount of remanent vortices pinned to surface roughness.

To nucleate the transition to potential flow, the turbulent flow must acquire a vortex configuration in which the turbulence can no longer be sustained. This requires that there are no unstable remanent vortices attached to the fork which would otherwise regenerate the turbulence. The mechanisms which dictate the likelihood of this are not understood and there is no firm theoretical prediction for how the average lifetime should vary with velocity. We have fitted the average lifetime to a form most recently used to fit vibrating sphere measurements [23], but various other forms can be used to generate equally good fits. For instance, two other forms were previously used to fit the same vibrating sphere data [21,33]. We also note that measurements of the average lifetime of turbulent flow around a vibrating wire resonator have been fitted to a function of the power dissipated by the turbulence [20]. In the latter experiments, the authors took specific measures to prepare the experiment in such a way that the wire in the potential flow state was relatively free of remanent vortices so turbulence could only be induced by injecting vortex rings from a nearby wire.

VII. SUMMARY AND CONCLUSIONS

In summary, we have made detailed measurements of the drag on a quartz tuning fork in superfluid ^{4}He at very low temperature. We have identified two characteristic velocities which separate three distinct regimes. For low velocity amplitudes $v < v_c$ there is stable potential flow with no measurable dissipation. At intermediate velocities $v_c < v < v^\star$ the potential flow state is quasistable while the turbulent state is unstable with an average lifetime which increases rapidly with increasing velocity. For higher velocities $v > v^\star$ the turbulent state is quasistable and the pure potential flow state is unstable with an average lifetime which decreases rapidly with increasing velocity.

We have presented a statistical study of the transitions between the two flow states. The potential flow to turbulent flow transition is qualitatively understood on the basis of remanent vortices pinned to surface roughness. The remanent vortices become mobile at high velocities and may eventually anneal away to increase the stability of potential flow. The turbulent flow to potential flow transition is dependent on the interplay between the surrounding vortex network of quantum turbulence and the vortices attached to the fork, some of which will be pinned by surface roughness. To better understand the transitions between different flow states, a quantitative model is needed which takes account of remanent vortices on rough surfaces and their dynamics in an alternating flow.

ACKNOWLEDGMENTS

We thank S. M. Holt, A. Stokes, and M. G. Ward for excellent technical support. This research is supported by the U.K. EPSRC and by the European FP7 Programme MICROKELVIN Project No. 228464.

[1] D. O. Clubb, O. V. L. Buu, R. M. Bowley, R. Nyman, and J. R. Owers-Bradley, J. Low Temp. Phys. **136**, 1 (2004).
[2] R. Blaauwgeers, M. Blazkova, M. Človečko, V. B. Eltsov, R. de Graaf, J. Hosio, M. Krusius, D. Schmoranzer, W. Schoepe, L. Skrbek, P. Skyba, R. E. Solntsev, and D. E. Zmeev, J. Low Temp. Phys. **146**, 537 (2007).
[3] D. I. Bradley, M. Človečko, S. N. Fisher, D. Garg, A. M. Guénault, E. Guise, R. P. Haley, G. R. Pickett, M. Poole, and V. Tsepelin, J. Low Temp. Phys. **171**, 750 (2013).
[4] M. Blažková, M. Človečko, E. Gažo, L. Skrbek, and P. Skyba, J. Low Temp. Phys. **148**, 305 (2007).
[5] D. I. Bradley, M. J. Fear, S. N. Fisher, A. M. Guénault, R. P. Haley, C. R. Lawson, P. V. E. McClintock, G. R. Pickett, R. Schanen, V. Tsepelin, and L. A. Wheatland, J. Low Temp. Phys. **156**, 116 (2009).
[6] M. Blažková, T. V. Chagovets, M. Rotter, D. Schmoranzer, and L. Skrbek, J. Low Temp. Phys. **150**, 194 (2008).
[7] D. I. Bradley, M. Človečko, E. Gažo, and P. Skyba, J. Low Temp. Phys. **152**, 147 (2008).
[8] D. I. Bradley, P. Crookston, S. N. Fisher, A. Ganshin, A. M. Guénault, R. P. Haley, M. J. Jackson, G. R. Pickett, R. Schanen, and V. Tsepelin, J. Low Temp. Phys. **157**, 476 (2009).
[9] A. Salmela, J. Tuoriniemi, and T. Rysti, J. Low Temp. Phys. **162**, 678 (2011).
[10] D. I. Bradley, M. Človečko, S. N. Fisher, D. Garg, E. Guise, R. P. Haley, O. Kolosov, G. R. Pickett, V. Tsepelin, D. Schmoranzer, and L. Skrbek, Phys. Rev. B **85**, 014501 (2012).
[11] D. Garg, V. B. Efimov, M. Giltrow, P. V. E. McClintock, L. Skrbek, and W. F. Vinen, Phys. Rev. B **85**, 144518 (2012).
[12] S. L. Ahlstrom, D. I. Bradley, M. Človečko, S. N. Fisher, A. M. Guénault, E. A. Guise, R. P. Haley, O. Kolosov, M. Kumar, P. McClintock, G. Pickett, E. Polturak, M. Poole, I. Todoshchenko, V. Tsepelin, and A. Woods, J. Low Temp. Phys. **175**, 140 (2014).

[13] J. Jäger, B. Schuderer, and W. Schoepe, Phys. Rev. Lett. **74**, 566 (1995).
[14] D. I. Bradley, D. O. Clubb, S. N. Fisher, A. M. Guénault, R. P. Haley, C. J. Matthews, G. R. Pickett, and K. L. Zaki, J. Low Temp. Phys. **138**, 493 (2005).
[15] H. Yano, A. Handa, H. Nakagawa, K. Obara, O. Ishikawa, T. Hata, and M. Nakagawa, J. Low Temp. Phys. **138**, 561 (2005).
[16] W. F. Vinen and J. J. Niemela, J. Low Temp. Phys. **128**, 167 (2002).
[17] Part label "KDS5M" from KDS America/Daishinku Corporation.
[18] D. I. Bradley, M. J. Fear, S. N. Fisher, A. M. Guénault, R. P. Haley, C. R. Lawson, G. R. Pickett, R. Schanen, V. Tsepelin, and L. A. Wheatland, J. Low Temp. Phys. **175**, 379 (2014).
[19] N. Hashimoto, A. Handa, M. Nakagawa, K. Obara, H. Yano, O. Ishikawa, and T. Hata, J. Low Temp. Phys **148**, 299 (2007).
[20] H. Yano, Y. Nago, R. Goto, K. Obara, O. Ishikawa, and T. Hata, Phys. Rev. B **81**, 220507 (2010).
[21] M. Niemetz and W. Schoepe, J. Low Temp. Phys. **135**, 447 (2004).
[22] W. Schoepe, J. Low Temp. Phys **161**, 526 (2010).
[23] W. Schoepe, J. Low Temp. Phys. **173**, 170 (2013).
[24] S. Holt and P. Skyba, Rev. Sci. Instrum. **83**, 064703 (2012).
[25] D. I. Bradley, P. Crookston, M. J. Fear, S. N. Fisher, G. Foulds, D. Garg, A. M. Guénault, E. Guise, R. P. Haley, O. Kolosov, G. R. Pickett, R. Schanen, and V. Tsepelin, J. Low Temp. Phys. **161**, 536 (2010).
[26] Y. Nago, A. Nishijima, H. Kubo, T. Ogawa, K. Obara, H. Yano, O. Ishikawa, and T. Hata, Phys. Rev. B **87**, 024511 (2013).
[27] W. I. Glaberson and R. J. Donnelly, Phys. Rev. **141**, 208 (1965).
[28] R. Hänninen, A. Mitani, and M. Tsubota, in *Proceedings of the 24th International Conference on Low Temperature Physics*, edited by Y. Takano, S. P. Hershfield, S. O. Hill, P. J. Hirschfeld, and A. M. Goldman, AIP Conf. Proc. No. 850 (AIP, Melville, NY, 2006), p. 217.
[29] M. Niemetz, H. Kerscher, and W. Schoepe, J. Low Temp. Phys. **126**, 287 (2002).
[30] C. Bäuerle, Y. M. Bunkov, S. N. Fisher, H. Godfrin, and G. R. Pickett, Nature (London) **382**, 332 (1996).
[31] V. Ruutu, V. Eltsov, A. Gill, T. Kibble, M. Krusius, Y. Makhlin, B. Placais, G. Volovik, and W. Xu, Nature (London) **382**, 334 (1996).
[32] M. Bartkowiak, S. N. Fisher, A. M. Guénault, R. P. Haley, G. R. Pickett, G. N. Plenderleith, and P. Skyba, Phys. Rev. Lett. **85**, 4321 (2000).
[33] W. Schoepe, Phys. Rev. Lett. **92**, 095301 (2004).